Journal of Naval Architecture and Marine Engineering
January, 2026
https://doi.org/10.3329/jname.v23i1.75864 *http://www.banglajol.info*

EXPERIMENTAL AND NUMERICAL INVESTIGATIONS OF THERMAL ANALYSIS DURING SUBMERGED ARC WELDING IN A BEAD-ON-PLATE OF MODIFIED 9CR-1MO STEEL

Abhijit Sarkar
Department of Mechanical Engineering, National Institute of Technology Goa, India-403703
Email: sarkarabhijit@nitgoa.ac.in

Abstract:

In the present study, a comprehensive experimental and numerical investigation has conducted to simulate and predict the thermal profile in weld joints of modified 9Cr-1Mo (P91) steel plates, with a particular focus on the influence of varying welding heat input. This study primarily investigates the thermal characteristics of the Submerged Arc Welding (SAW) process using a moving heat source model based on a Gaussian distribution. A methodology based on the Finite Difference Method (FDM) is developed and implemented using MATLAB to accurately estimate the thermal profile. The results show good agreement between the numerical and experimental data, with an overall error ranging between 6% to 9%, thereby confirming the accuracy and reliability of the proposed numerical model. Finally, the results emphasize the critical role of welding parameters in shaping the thermal profile. It has observed that increasing the welding current, while maintaining a constant welding speed, has resulted in higher heat input and elevated weldment temperatures. The peak temperatures have recorded as 155°C, 198°C, and 210°C at welding speeds of 0.60 m/min, 0.75 m/min, and 0.90 m/min, respectively. A maximum percentage difference of 7% has found between the experimental and numerical results, further validating the accuracy of the proposed model.

Keywords: Submerged Arc Welding (SAW) process, modified 9Cr-1Mo steel, Gaussian distribution moving heat source model, Finite Difference Method (FDM), bead-on-plate welds.

NOMENCLATURE

SAW	Submerged Arc Welding	*T*	Temperature (°C)
FDM	Finite difference method	*t*	Time (sec)
HAZ	Heat Affected Zone	*q*	Heat flux intensity (W/m²)
FEA	Finite Element Analysis	*Cp*	Specific heat (J/kg°C)
FVM	Finite Volume Method	*Q*	Total power of the heat source (W)
TIG	Tungsten Inert Gas Welding	*r*	Radius of the heat source (mm)
GTA	Gas Tungsten Arc	r^{-}	Average radial distance from the centre of the
FEM	Finite element method	*exp*	Exponential function.
I	Welding Current	*Vs*	Welding speed (m/s)
S	Welding speed	*x,y,z*	Coordinates of the heat source.
N	Stick Out	***Greek symbols***	
DAQ	Data Acquisition	*ρ*	Density of Material (kg/m³)
T1, T2, T3,T4&T5	Thermocouple numbers	α	Co-efficient of thermal expansion
k	Thermal conductivity of material (w/(m^0 C))		

1. Introduction

Steel is the most commonly used material for welded fabrications. Cr-Mo steel is particularly suitable for making heavy-duty products that operate under high-temperature conditions. Therefore, it is important to consider the welding characteristics of P91 when choosing a welding method. Research has shown that P91 can be satisfactorily welded using various processes, including manual metal arc, submerged arc, and gas tungsten-

  Received: Sept., 2024

arc welding (Arivazhagan et al, 2013). More than forty years ago, the first reported model for stationary and dynamic heat sources was developed and frequently used in many manufacturing processes (Ghosh et al, 2011). During the welding process, the heat source plays a crucial role in determining the weld bead geometry, the width of the Heat Affected Zone (HAZ), distortion, and residual stress (Zubairuddin et al, 2014). With the aid of simulation software and code, numerical techniques can be understood, and the thermal cycles can be predicted with reasonable accuracy for the complex phenomena of fusion welding (He, 2012). A multitude of numerical and mathematical models has developed to forecast temperature distributions in welded joints (Biswas et. al, 2010; Nart et al, 2013 and Yaghi et al, 2009). Firstly, Rosenthal (1941) and (1946) derived an analytical model to predict the temperature for steady state, two-dimensional heat flow problems in welding. When it comes to welding, there are many challenges due to complex shapes and varying heat conditions that cannot be solved using traditional mathematical methods. In these situations, computers can provide accurate approximate solutions through numerical methods. By using advanced numerical programs and methods, precise and dependable results can be achieved. (Sarkar et al, 2015).

In various thermal and mechanical calculations, a numerical model called the Finite Difference Method (FDM) is frequently used due to its simplicity and speed, particularly for simple geometries. It is feasible to reduce the extensive computer time needed for 3D cases. Several researchers have noted that FDM can address challenges encountered in numerical methods such as Finite Element Analysis (FEA), Finite Volume Method (FVM), and others (Mazumder and Steen, 1980; Pilipenko, 2001). In 1980, Sharir et al. (1980) introduced the finite difference method to calculate the unsteady heat flow during the fusion welding of thin tantalum sheets. Al-Sa'ady et al. (2011) proposed using the finite difference method to calculate time-dependent temperature distributions during the arc welding of low-carbon steel. They have shown that the Finite Difference Method outperforms empirical models by capturing comprehensive thermal and mechanical influences on weld joint formation. Yeh et al, (2003) examined the steady-state temperature profiles of aluminum plates welded by gas tungsten using the finite difference method. They found that the temperature of the welded plate rises with higher heat input, while increased welding speed has the opposite effect. Additionally, they observed that the calculated temperatures of the weldments increase with higher preheating levels. In their study, Ghadimi et al, (2013) utilized the three-dimensional finite difference method to obtain thermal history curves and cooling times for single-pass underwater wet weldments. Their findings indicated that convective heat transfer is more impactful than radiation in temperature calculations, suggesting that radiation can be disregarded. Boo and Cho (1990) conducted a study on obtaining transient temperature distributions in a plate of finite thickness. They have successfully solved a transient three-dimensional heat conduction equation with convection boundary conditions applied at the surfaces of the weldment during arc welding.

Rothwell and Abson (2013) investigated the impact of welding thermal history on the mechanical properties of grade 91 steel weldments. Grill (1982) conducted a study on the heat flow of welding during girth welding using the TIG method. In the study, a mathematical model was presented for calculating the three-dimensional thermal history of a composite cylinder using the implicit finite difference method. Kou et al, (1983) developed a numerical method for three-dimensional heat flow using a finite-difference model to analyse the impact of a moving heat source in a semi-infinite body. Dill (1997) studied the thermal history of single-pass underwater weldments and employed the three-dimensional Crank–Nicolson finite difference method to solve the heat transfer equations. His model incorporated the Adams approach and the semi-empirical correlation developed by Tsai and Masubuchi to determine weldment temperatures during welding. Kumar et al, (2019) investigates the MHD Cattaneo-Christov flow of Carreau fluid over a melting surface with variable thickness using transformed ordinary differential equations (ODEs) solved via the shooting and Runge–Kutta fourth methods, revealing that nonuniform heat source parameters significantly influence heat transfer characteristics.

Zubairuddin et al. (2008) has conducted a numerical simulation to analyze the thermal cycles of Grade P91 steel during autogenous GTA welding using FEM. Zubairuddin et al. (2024) has conducted a FEM-based thermo-mechanical analysis using SYSWELD to compare GTA and LASER welding processes on 2 mm thick Grade 91 steel plates, finding that LASER welding resulted in lower residual stress and distortion than GTA welding under similar heat input conditions. Zubairuddin et al. (2025) performed FEM-based thermo-mechanical analysis of P91 steel butt joints welded using A-TIG and conventional TIG processes, concluding that A-TIG resulted in lower residual stress, reduced distortion, and deeper, narrower weld penetration, with predictions closely matching experimental measurements. Attarha et al. (2011) conducted a study on the distribution of welding temperature in a thinly welded plate using experimental and finite element simulation. In their

investigation, Abhijit et al. (2015) developed a numerical model to analyze the impact of welding parameters on temperature variations in the Submerged Arc Welding process (SAW). They utilized a moving heat source model (Gaussian distribution) and the finite difference method (FDM) and found a strong agreement between experimental and numerical results, confirming the capability and reliability of the proposed numerical model. It also highlighted the significant role of process parameters in influencing temperature distribution.

Although several studies have addressed the analytical and computational thermal analysis of various welding processes and materials, research on the welding of P91 steel using the Submerged Arc Welding (SAW) process remains limited. It requires precise control of heat input, as it directly influences the thermal cycle and is responsible for cracking, hardness variations, and potential metallurgical degradation. SAW has high heat input, which can lead to undesirable microstructures in P91 if not well controlled. This paper has aimed to use the Finite Difference Method (FDM) to simulate heat transfer in welding, specifically focusing on modified 9Cr-1Mo steel during the SAW process. The temperature fields and thermal cycle simulations have carried out using MATLAB code. The proposed approach has employed to perform thermal analysis on 12 mm thick P91 steel, considering varying process parameters, and the results have experimentally validated. Additionally, nine bead-on-plate welds have conducted experimentally to examine the characteristics of thermal profiles through thermocouple measurements. Furthermore, the impact of process parameters and heat input on thermal profiles has investigated using the developed numerical simulation method.

2. Materials and Methods:

This research work has mainly addressed the following aspects:
a) Exploring how different welding conditions have impacted the experimental thermal history and the associated experimental process.
b) Developing a numerical model using the finite difference technique to solve the governing heat transfer equation. This model has used to analyze the temperature distribution resulting from heat flow and to predict variations in the thermal profile as welding parameters have changed.
c) Validating and comparing both numerical and experimental results under various welding conditions.
The program outline for this study has presented in Figure 1 and is further described in the following sections.

2.1. Selection of welding process, material, electrode wire and flux:

2.1.1. Welding process:

The Submerged Arc Welding (SAW) process has chosen for this investigation due to its high productivity, low production cost, and ability to accommodate a wide range of welding currents and speeds. It has also recognized its potential to be automated, enabling consistent production of defect-free welds.

2.1.2. Material:

A material known as P91 (Grade 91), which belongs to the modified group of Cr–Mo steels, has been selected for this investigation. It has provided by NIPPON Ltd. The steel plate used has had dimensions of 12 mm thickness, 200 mm length, and 100 mm width. The base plates have been normalized at 1080 °C for 1 hour and tempered at 760 °C for 2 hours

2.1.3. Electrode wire and flux:

For the Submerged Arc Welding (SAW) process, an AWS SFA 5.23 electrode wire (Ø3.15 mm), matching the composition of the base plate, has been used. It has supplied by D&H Scheron Electrodes Pvt. Ltd. The flux used for welding has been Max-Flux SAF12, with a basicity index of 3.1. For detailed chemical composition and mechanical properties, please refer to Tables 1 and 2.

2.2. Standardization of the welding process parameters:

The chosen ranges of physical factors, such as welding current (I), welding speed (S), and nozzle-to-plate distance (N) are appropriate because they are based on a combination of literature survey, preliminary analysis, and experimental trial runs, ensuring that the selected values are both practically viable and technically relevant for producing high-quality welds in the given material and process setup. The standardization process also

considers industry practices and recommendations for the specific welding technique (e.g., SAW), making the selected parameter ranges well aligned with real-world applications and presented in Table 3.

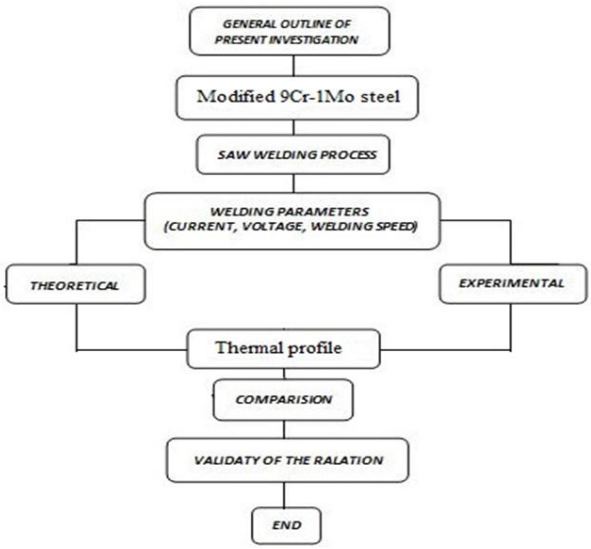

Fig. 1: General outline of the present investigation.

Table 1: Chemical composition (wt %) of the base plate of modified 9Cr-1Mo (P91) (spectroscopy analysis) and electrode wire.

Element	**C**	**Mn**	**P**	**S**	**Cr**	**Ni**	**Mo**	**Nb**
Modified 9Cr-1Mo (P91) steel	0.105	0.432	0.014	0.0008	8.975	0.228	0.855	0.075
	Al	**V**	**C_{eq}**	Fe				
	0.013	0.202	-	rest				
Filer consumable	**C**	**Mn**	**P**	**S**	**Cr**	**Ni**	**Mo**	**Nb**
	0.0105	0.432	0.014	0.0008	8.975	0.228	0.855	0.075
	Al	**V**	**C_{eq}**					
	0.013	0.202	-					

Table 2: Mechanical properties of modified 9Cr-1Mo (P91) steel.

Materials	Tensile strength (N/mm^2)	Hardness HV 10	Toughness (J)	Elongation % (mm),
Modified 9Cr-1Mo (P91) steel	693.74	230	63.5	20

2.3 Developing the design matrix of experiments

The current study has used Taguchi's L9 orthogonal array with three variables such as welding current (I), welding speed (S), and stick-out or nozzle-to-plate distance (N) at three levels (I: 400 to 550 A, S: 0.60 to 0.90 m/min, and N: 20 to 25 mm) to limit the total number of experiments. This approach has allowed the variation of process parameters to assess weld quality while minimizing the number of experiments conducted, using three levels of variation (Tarng et. al, 2002; Datta et. al 2008; Biswas et. al, 2010). With Taguchi's L9 orthogonal array, only nine experiments have been required, and the details of the experimental design have provided in Table 4.

Table 3: Welding process parameters and their levels of modified 9Cr-1Mo (P91) steel.

Sl. No.	Parameters	Notations	Units	Materials	
				Modified 9Cr-1Mo (P91) steel	
				Levels	
				Lower limits	Higher limits
1	Welding Current	I	Amp	400	550
2	Welding speed	S	m/min	0.60	0.90
3	Stick Out	N	mm	20	25

Table 4: Design of Experiments of process parameters with coded and uncoded.

Exp No.	Coded variable			Actual variable		
	Welding current (I)	Welding speed (S)	Stick out (N)	Welding current (Amp)	Welding speed (m/min)	Stick out (mm)
1	1	1	1	400	0.60	20
2	1	2	2	400	0.75	22
3	1	3	3	400	0.90	25
4	2	1	2	500	0.60	22
5	2	2	3	500	0.75	25
6	2	3	1	500	0.90	20
7	3	1	3	550	0.60	25
8	3	2	1	550	0.75	20
9	3	3	2	550	0.90	22

2.4 Preparation of the test plate and positioning of thermocouples

The test plates have finished by sharpening with a minimal depth of cut and feed rate to ensure that there have been no changes in the microstructure. Prior to welding, all edges have been thoroughly cleaned using mechanical and chemical methods to prevent any potential sources of contamination such as rust, scale, dust, oil, or moisture, which could have led to weld defects. After cleaning the plate, K-type chromel-alumal thermocouples (Rahul et. al, 2014) (specification: temperature range of -200 °C to +1350 °C) have been securely fixed by drilling holes and inserting the thermocouples at specific locations in the X and Y directions. Care has taken to position the thermocouple centrally, with its tip near the end of the drilled hole. The schematic diagram (Fig. 2) has illustrated the positions on the plate where the thermocouples have attached at a depth of 0.6 cm. The depths of the thermocouples have been determined based on cross-sections taken from preliminary welds made under specified conditions. The positions of the thermocouples, based on the chosen coordinate system, have listed in Table 5.

2.4.1. Data acquisition device

A PC-based data acquisition system (NI PCIE-6351, X Series Multifunction DAQ) with a maximum sampling frequency of 100 MHz (as shown in Figure 3) has employed in this study. The system has functioned as a multi-channel digital data logger integrated with precision sensors to monitor key parameters—voltage, current, and temperature—in real time. High-accuracy Type K thermocouples have been used for temperature measurements (±1.0 °C), a calibrated shunt resistor has been employed for current sensing (±0.2%), and a precision voltmeter has recorded voltage (±0.1% of full-scale reading). All sensors have interfaced with the DAQ unit via a LabVIEW-based control panel, enabling continuous data acquisition and real-time visualization. The system has configured to sample at an optimized rate to maintain adequate temporal resolution while avoiding redundant data collection. Prior to testing, the setup has been calibrated using standard reference instruments to ensure measurement accuracy. Each measurement has repeated three times to confirm repeatability and minimize random errors.

Table 5: The dimension of the position of the thermocouple in the welded plate.

Thermocouple (k-type) (chromul-Aumul)	position (cm)		
	X	Y	Z
T1	10	0.6	0.6
T2	10	0.8	0.6
T3	10	1.0	0.6
T4	8	0.6	0.6
T5	6	0.6	0.6

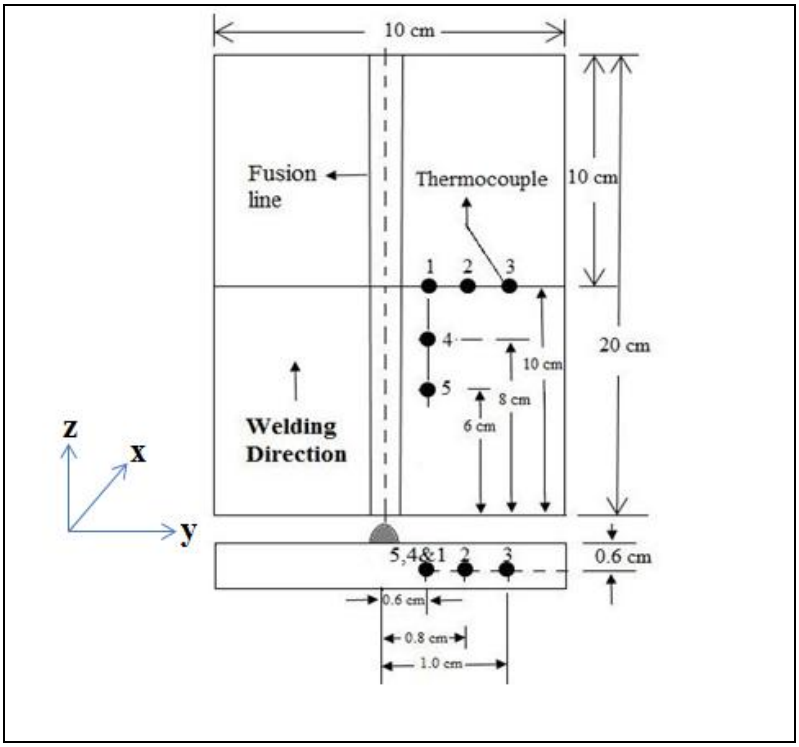

Fig. 2: Position of the thermocouples in the welded plate.

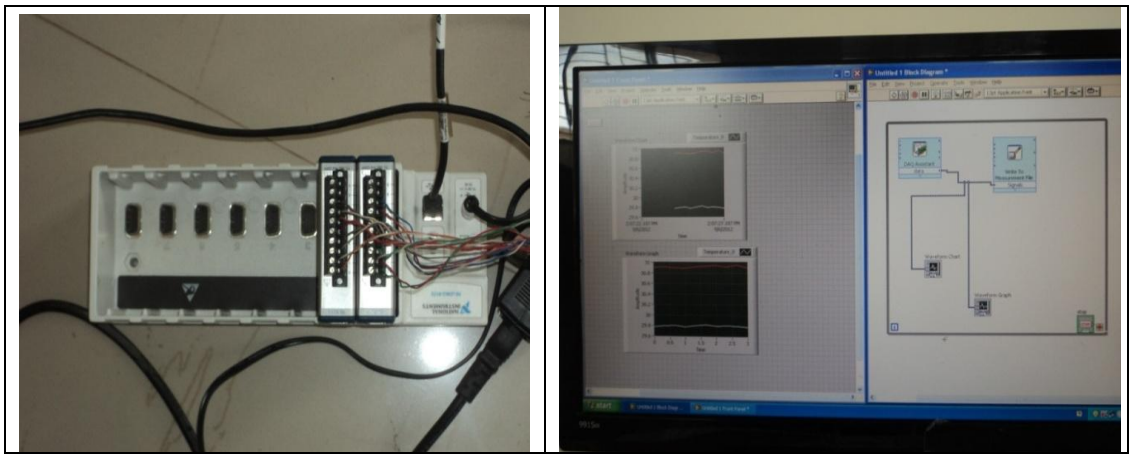

Fig.3: Data acquisition device setup.

2.5. Welding procedure

The experiment has conducted using the SAW machine at ADOR WELDING LTD. in India, Machine No: MODEL PS-1200(F), as shown in Figure 4. Once the welding parameters have standardized using the design matrix, welding has performed on each of the plates. The standard procedure has involved laying a bead on the plate to study heat transfer in the welded plate. To ensure only stable welding conditions over the test plate, starting and run-off plates have used. The temperatures have been continuously recorded using thermocouples and have collected by the LabVIEW Data Acquisition system.

Fig. 4: SAW machine (MODEL PS-1200(F)) setup.

3. Numerical Approach

With the knowledge of heat flux distribution, it is now necessary to calculate the temperature distribution at any point on the weldment during welding. This requires solving the following governing unsteady state heat transfer equation:

$$\frac{\partial}{\partial x}\left(k\frac{\partial T}{\partial x}\right)+\frac{\partial}{\partial y}\left(k\frac{\partial T}{\partial y}\right)+\frac{\partial}{\partial z}\left(k\frac{\partial T}{\partial z}\right)+q(r)=\rho c_p\frac{\partial T}{\partial t} \tag{1}$$

In this current study, a Gaussian-distributed conical heat source is utilized to simulate the temperature distribution in the weldment, and the following equation is used.

$$q(r)=\frac{3Q}{\pi\bar{r}^2}exp\left[-3\left(\frac{r}{\bar{r}}\right)^2\right]exp\left[-3\left(\frac{x-v_s t}{\bar{r}}\right)^2\right] \tag{2}$$

To fully describe the mathematical model, it is determined by initial and boundary conditions as well as the thermal properties of weldments (refer to Table 6).

Table 6: Thermal physical properties of modified 9Cr-1Mo (P91) steel (Yaghi et. al, 2009).

Temper -ature (^{0}C)	Thermal conductivity (W/mK)	Liquiduste -mperature (^{0}C)	Solidus temperatur e (^{0}C)	Thermal expansion coefficient (10-6/K)	Specific heat (J/kg.K)	Density (kg/m^3)	Latent heat (kJ/kg)
20	26	1500	1420	10.4	440	7770	260

3.1. Computer implementation

The equation (Equ. 2) that controls the heat flow in the weldment described above is implemented using a MATLAB code based on the finite difference technique (Anantha et. al, 2020) which takes into account all the boundary conditions and initial conditions. When solving time-dependent partial differential equations (PDEs) like the heat conduction equation, the Finite Difference Method (FDM) is used to discretize space, reducing the PDE into a system of ordinary differential equations (ODEs) in time. Discretize Space Using FDM:

$$\frac{dT_i}{dt} = \propto \frac{T_{i+1} - 2T_i + T_{i-1}}{\Delta x^2} \tag{3}$$

The logic for converting the mathematical procedure into a computer program is broken down into various stages for easy understanding and implementation on a computer. During welding, the welding source moves parallel to 'x' direction with welding speed of Vs and ζ represents a moving abscissa, which is parallel to x axis in weldments as shown in figure 5. A reference section is taken at a distance of 100 mm from starting point of welding, which is related with ζ. A careful check for the mesh and grid independence of our numerical solutions has made to ensure the accuracy and validity of the numerical schemes. For this purpose, in mesh systems, t=0.05 s and y= z= 2 mm, is tested. Spatial increment y, and z of 1mm, and a time step t=0.025 s are thus adopted in the calculation.

4. Results and Discussion

The results of the experimentation have shown the temperature distribution in the weldment, plotted as thermal profiles both along and transverse to the welding direction (in Fig. 6). Theoretical thermal profiles have developed using numerical methods, and have validated by comparing them with the experimental results. The effects of welding current and speed on heat flow and temperature distribution have also described.

During the SAW process, five thermocouples have recorded transient temperatures. These thermocouples have connected to a data acquisition (DAQ) system, which has in turn attached to a personal computer running a customized program developed in LabVIEW software. Based on the recorded data, experimental thermal profiles have drawn for all nine parametric settings. A plot, corresponding to a welding current of 400 A and a welding speed of 0.6 m/min, has provided in Fig. 6 for discussion.

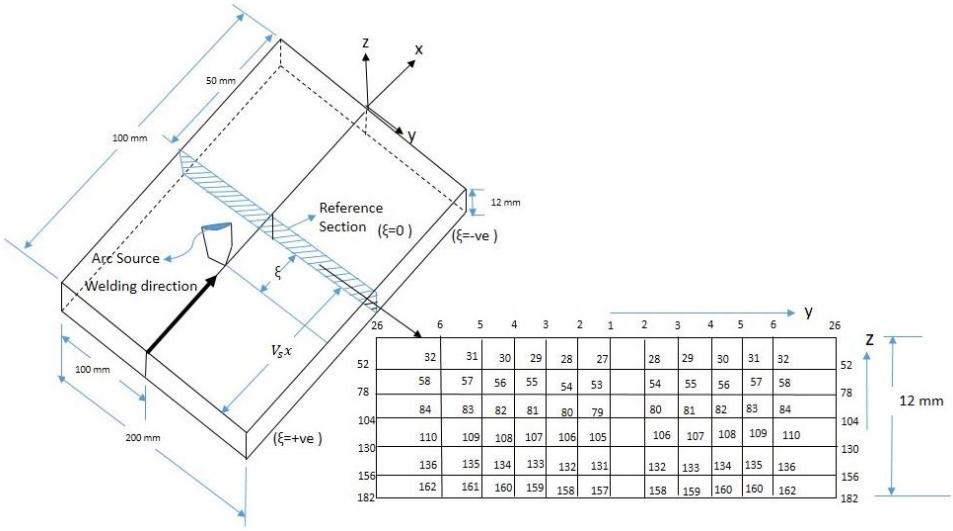

	26	6	5	4	3	2	1	2	3	4	5	6	26	
52	32	31	30	29	28	27		28	29	30	31	32	52	
78	58	57	56	55	54	53		54	55	56	57	58	78	
104	84	83	82	81	80	79		80	81	82	83	84	104	
130	110	109	108	107	106	105		106	107	108	109	110	130	
156	136	135	134	133	132	131		132	133	134	135	136	156	
182	162	161	160	159	158	157		158	159	160	160	162	182	

Fig: 5: Dimensions of weld (all dimensions in mm) plate and discretization of plate section

The nature of the thermal profile has indicated the heating cycle, peak temperature, and cooling cycle. The figure has shown that thermocouples placed along the longitudinal direction (T5, T4, and T1) have exhibited the same peak temperature, but the time to reach this temperature has differed. This has occurred because the welding heat source, despite delivering the same heat input, has reached each thermocouple location at different times.

Conversely, thermocouples placed in the transverse direction (i.e., at T1, T2, and T3) have shown different peak temperatures. The peak temperature has decreased from the weld centreline to locations farther from the centreline. The time taken to reach the peak temperature has remained nearly the same for all positions, due to the high heat input near the source, which has gradually diminished with increasing distance. It has also observed that the thermocouple positioned closest to the heat source has displayed a distinct thermal profile compared to those located farther away, indicating significantly higher temperatures near the heat source.

Temperatures have become nearly equal on the cooling side away from the weld centreline, indicating a transient temperature gradient near the heat source. Additionally, the thermal profiles at different positions have shown similar trends, suggesting that the weldment has heated up in a shorter time. Similar trends have observed under other welding conditions.

The proposed numerical model, based on the finite difference technique, has provided theoretical thermal profiles for different locations within the weldment. These profiles have obtained under varying welding conditions. To generate the theoretical thermal profiles for a specific location, the necessary data have been extracted from a computer printout corresponding to a set of welding conditions (welding current of 500 A and welding speed of 0.9 m/min), and have been plotted in Fig. 7.

The figure has indicated that locations placed along the longitudinal direction or welding direction (i.e., T1, T4, and T5) have exhibited the same peak temperature, although the time to reach this temperature has varied. It has also observed that the peak temperature has shifted as the heat source has progressed along the welding direction. Each node has reached its peak temperature when the heat source has arrived and has begun to cool once the source has moved past.

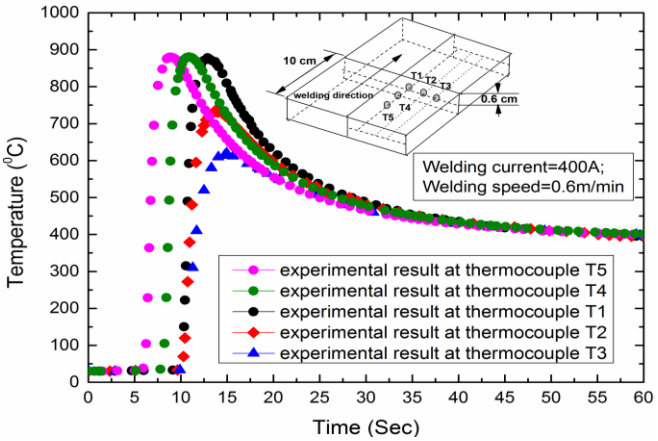

Fig. 6: Thermal profiles generated for a welding current of 400A and welding speed of 0.6 m/min

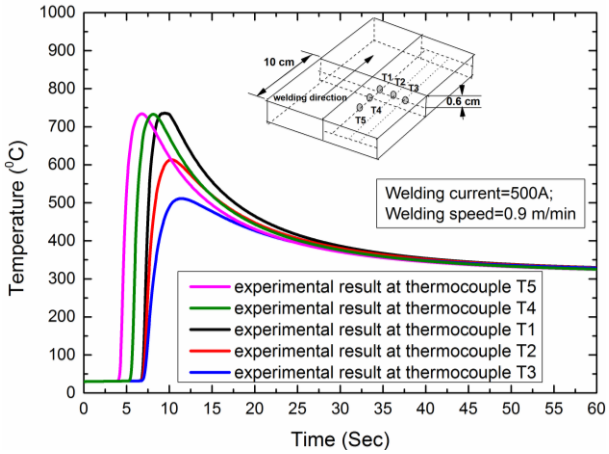

Fig. 7: Thermal profiles in the longitudinal and transverse direction in weldment of welding current 500A and a welding speed of 0.9 m/min.

Conversely, locations positioned in the transverse direction (T1, T2, and T3) have displayed different peak temperatures, with the peak temperature decreasing as the position has moved away from the weld centerline (i.e., in the x-direction). However, the time required to achieve the peak temperature has remained nearly the same for a constant welding speed with varying welding currents. Similar trends have observed under other welding conditions as well.

4.1 Effect of current on temperature distribution

In order to study the impact of welding current on the temperature distribution of the weldment, the welding speed is kept constant. By maintaining a consistent welding speed and varying the current from 400A to 550A, the corresponding thermal profiles for 8mm from the welding line are plotted in Fig. 8 (A-C). These figures demonstrate that an increase in current leads to a higher peak temperature with constant welding speed (Sarkar et. al, 2015). Additionally, the change in current from 400A to 550A at a constant speed results in an estimated overall percentage change in temperature of 15-20%

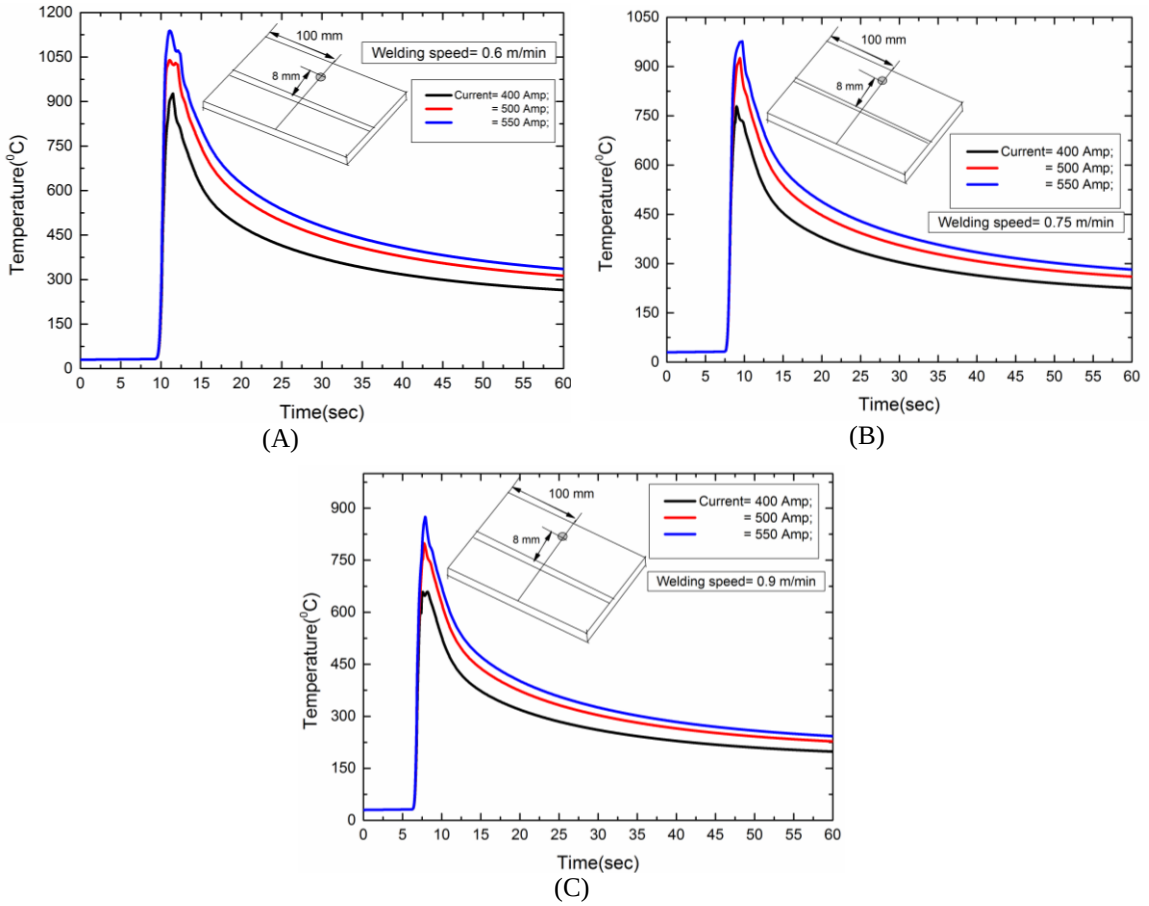

Fig.8: Thermal profiles vary current with constant welding speed.

4.2. Effect of welding speed on temperature distribution:

In the diagrams labelled Fig.9 (A-C), thermal profiles are depicted along the thermocouple position T3 (10 mm) in the transverse direction of the weldment. These profiles vary with the welding speed (0.60 - 0.90 m/min) for a constant current (400A, 500A, or 550A). From the figures, it is evident that as the welding speed increases, the heat source has less time to interact with the workpiece, resulting in a decrease in the maximum temperature at a specific point. Therefore, at a slower speed, the peak temperature is higher compared to a faster speed. The attainment of the peak temperature also varies depending on the welding speed. With a faster speed, as the materials is heated in a shorter time, it becomes challenging to differentiate or resolve the peak temperature for various speed increases. This observation aligns with findings by others (Ahmed and Jarvis, 1996; Alwan, 2011). The thermal profiles indicate that the maximum or peak temperature obtained varies between 155°C, 198°C, and 210°C for welding speeds ranging from 0.60 m/min to 0.90 m/min for constant currents (400A, 500A, and 550A) with overall percentage change in temperature of 10-13%. Additionally, the temperature range between 700 °C and 900 °C is critical in welding processes due to its influence on microstructural transformations and mechanical properties, and as indicated by the thermal profiles. several parameters, including welding speed, which affects the heat interaction time and thus the peak temperature (with slower

speeds like 0.60 m/min allowing greater thermal exposure compared to faster speeds like 0.90 m/min); welding current, where higher values (400A, 500A, and 550A) provide greater heat input and increase the likelihood of reaching or exceeding this temperature range; the combined effect of current and speed, which defines the net heat input and energy density necessary for crossing the 700–900 °C threshold; the material's thermal conductivity and its ability to dissipate heat, with lower conductivity promoting higher local temperatures; and the thermocouple's measurement location (T3, 10 mm from the weld centreline), where reaching this range reflects significant heat transfer collectively govern the occurrence and extent of temperatures within this critical range

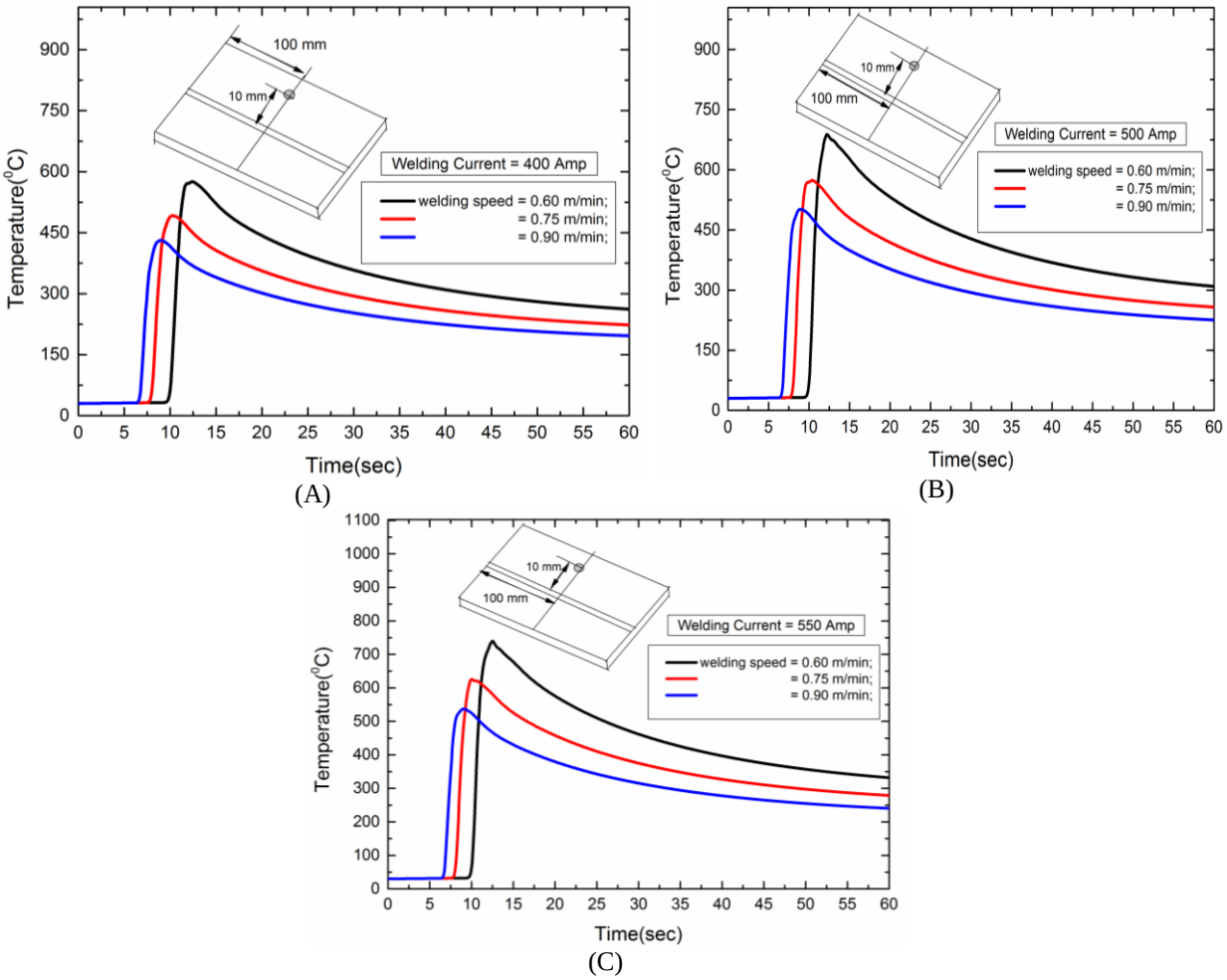

Fig.9: Thermal profiles for different values of welding speed with constant welding current.

4.3 Comparison of thermal profiles of experimental and numerical result

The experimental thermal cycles at monitoring locations T1, T2, and T3 are compared with numerical data using welding currents of 400A, 500A, and 550A, and welding speeds of 0.6m/min, 0.75m/min, and 0.9m/min. A comparison between the theoretical predictions and experimental observations revealed a strong agreement, validating the accuracy of the developed model, with the overall percentage error found to lie within the range of 6% to 9%, indicating reliable and consistent performance across the evaluated conditions as illustrated in Fig. 10 (A–D).

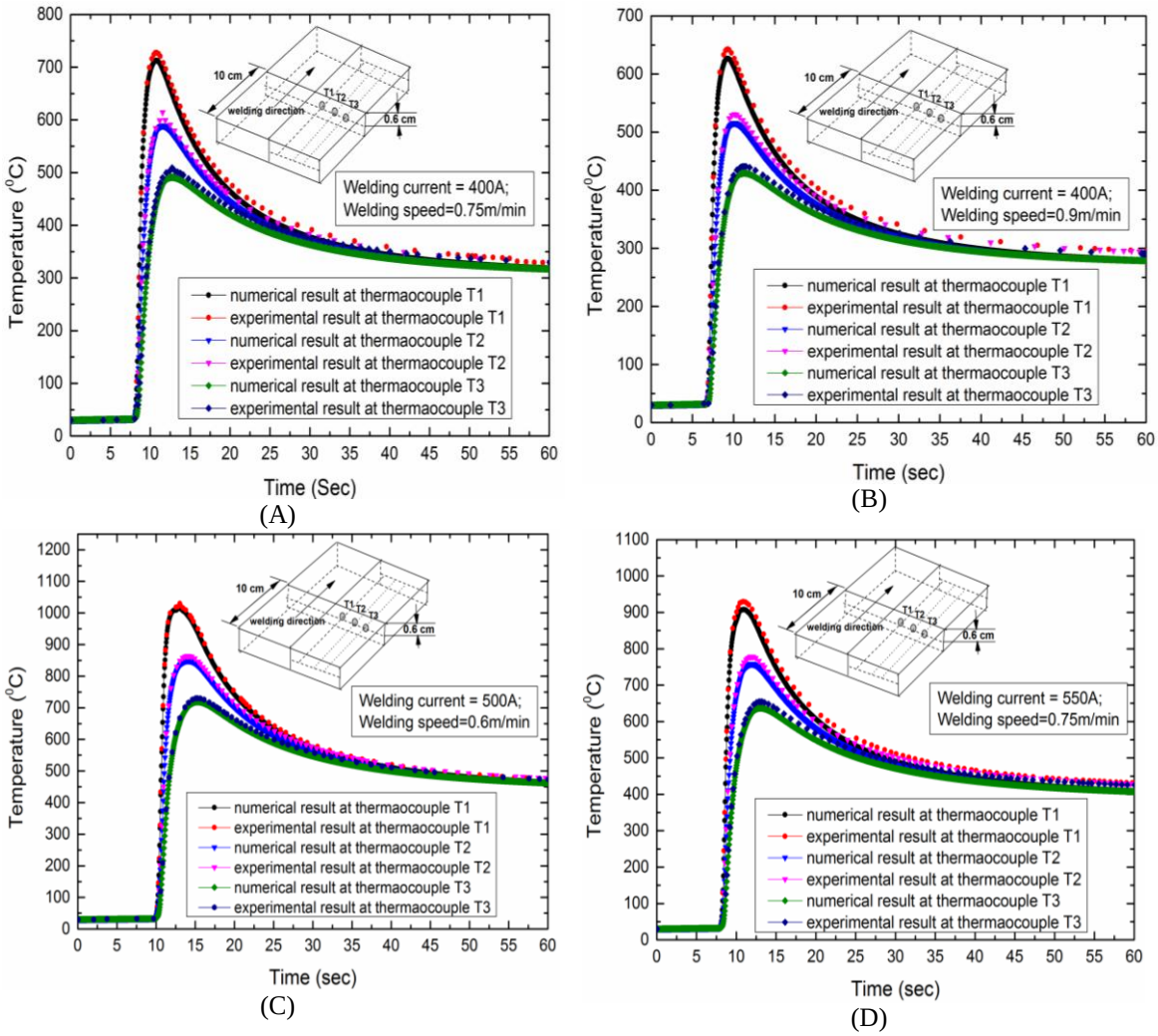

Fig.10: Validation of thermal profiles for numerical results with experimental results

5. Conclusions

An analysis of temperature distribution in P91 weldments during the Submerged Arc Welding (SAW) process has carried out using multiple thermocouples placed in both transverse and axial directions. The study has revealed that variations in welding parameters, such as welding current and speed, have significantly influenced the total heat input and, consequently, the resulting thermal profiles. These variations have successfully predicted using a Finite Difference Method (FDM)-based heat source fitting analysis. The developed computational model has proven to be both efficient and accurate for the proposed thermo-modelling approach. A comparison between the theoretical and experimental results has demonstrated a strong correlation, with an overall error ranging between 6% and 9%. Furthermore, the study has found good agreement between the predicted and experimentally measured thermal cycles for the bead-on-plate weldments. It has concluded that higher heat input, especially from increased welding current at constant speed, has resulted in elevated temperatures within the weldment. With an increase in welding current while maintaining a constant welding speed, the peak temperature also increased. The maximum percentage difference between the experimental and numerical results is observed to be 7%. The study also found that the maximum temperatures obtained are 155 °C, 198 °C, and 210 °C for welding speeds of 0.60 m/min, 0.75 m/min, and 0.90 m/min, respectively, at constant welding current. The proposed method holds potential for future applications in selecting welding processes and parameters tailored to meet the thermal demands of specific design requirements.

CRediT Author Statement

Dr. Abhijit Sarkar: Conceptualization, Methodology, Validation, Analysis, Investigation, Writing – Original Draft, Writing – Review and Editing, Visualization conceptualization, experimentation and manuscript preparation.

Acknowledgements

The authors gratefully acknowledge NIT Agartala for support during the experimental work. Authors also are thankful to NIT Goa for assisting in the work.

References

Ahmed N. U. and Jarvis B. L (1996). Thermal cycles in submerged multiple electrode arc welding. Welding Research Supplement, 15-23.
https://s3.us-east-1.amazonaws.com/WJ-www.aws.org/supplement/WJ_1996_01_s15.pdf
Al-Sa'ady, M. H., Abdulsattar, M. A., and Al-Khafagy, L. S. (2011). Finite difference simulation of low carbon steel manual arc welding. Thermal Science, 15(1), 207-214. https://doi.org/10.2298/TSCI100206055S
Alwan, D. A. S. (2011). Reliability of numerical analysis of cooling curves in the fusion zone of submerged arc welding (saw) process. The Iraqi Journal for Mechanical and Material Engineering, 11, 672-682. https://iasj.rdd.edu.iq/journals/uploads/2024/12/23/dbac87e0ed9c36d426bcb1cc398044f8.pdf
Arivazhagan, B., and Vasudevan, M. (2013). A study of microstructure and mechanical properties of grade 91 steel A-TIG weld joint. Journal of materials engineering and performance, 22(12), 3708-3716. https://doi.org/10.1007/s11665-013-0694-9
Attarha, M. J., and Sattari-Far, I. (2011). Study on welding temperature distribution in thin welded plates through experimental measurements and finite element simulation. Journal of Materials Processing Technology, 211(4), 688-694. https://doi.org/10.1016/j.jmatprotec.2010.12.003
Biswas, P., Mahapatra, M. M., and Mandal, N. R. (2010). Numerical and experimental study on prediction of thermal history and residual deformation of double-sided fillet welding. Proceedings of the Institution of Mechanical Engineers, Part B: Journal of Engineering Manufacture, 224(1), 125-134. https://doi.org/10.1243/09544054JEM1666
Boo, K. S., and Cho, H. S. (1990). Transient temperature distribution in arc welding of finite thickness plates. Proceedings of the Institution of Mechanical Engineers, Part B: Journal of Engineering Manufacture, 204(3), 175-183. https://doi.org/10.1243/PIME_PROC_1990_204_005_01
Datta S, Bandyopadhyay A, Pal PK (2008). Application of Taguchi philosophy for parametric optimisation of bead geometry and HAZ width in submerged arc welding using a mixture of fresh flux and fused flux. Int J AdvManufTechnol 36:689-698 https://doi.org/10.1007/s00170-006-0894-7
Dill, J. F. (1997). Model for Estimation of Thermal History Produced by a Single Pass Underwater Wet Weld, Doctoral Dissertation, Monterey, California Naval Postgraduate School.
Ghadimi, P., Ghassemi, H., Ghassabzadeh, M., and Kiaei, Z. (2013). Three-dimensional simulation of underwater welding and investigation of effective parameters. Welding journal, 92(8).
Ghosh, A., Chattopadhyaya, S., and Das, R. K. (2011). Effect of heat input on submerged arc welded plates. Procedia Engineering, 10, 2791-2796. https://doi.org/10.1016/j.proeng.2011.04.464
Grill, A. (1982). The thermal history of a composite cylinder girth welded by TIG. International Journal for Numerical Methods in Engineering, 18(7), 1031-1044. https://doi.org/10.1002/nme.1620180707
He, X. (2012). Finite element analysis of laser welding: a state of art review. Materials and Manufacturing Processes, 27(12), 1354-1365. https://doi.org/10.1080/10426914.2012.709345
Kumar, K.A., Ramana Reddy, J. V., Sugunamma, V., and Sandeep, N. (2019, February). MHD Carreau fluid flow past a melting surface with Cattaneo-Christov heat flux. In Applied mathematics and scientific computing: International conference on advances in mathematical sciences, vellore, India, december 2017-volume II (pp. 325-336). Cham: Springer International Publishing. https://doi.org/10.1007/978-3-030-01123- 9_32
Kumar, K.A., Sugunamma, V., and Sandeep, N. (2020). Influence of viscous dissipation on MHD flow of micropolar fluid over a slendering stretching surface with modified heat flux model: K. Anantha Kumar et al. Journal of Thermal Analysis and Calorimetry, 139(6), 3661-3674. https://doi.org/10.1007/s10973-019-08694-8
Kou, S., Sun, D. K., and Le, Y. P. (1983). A fundamental study of laser transformation hardening. Metallurgical Transactions A, 14(3), 643-653. https://doi.org/10.1007/BF02643780

Mazumder, J., and Steen, W. M. (1980). Heat transfer model for CW laser material processing. Journal of Applied Physics, 51(2), 941-947.https://doi.org/10.1063/1.327672
Nart, E., and Celik, Y. (2013). A practical approach for simulating submerged arc welding process using FE method. Journal of constructional steel research, 84, 62-71. https://doi.org/10.1016/j.jcsr.2013.02.005
Pilipenko, A. (2001). Computer simulation of residual stress and distortion of thick plates in multielectrode submerged arc welding: their mitigation techniques. https://nva.sikt.no/registration/0198cc97f7ac-c1ed0056-a1aa-4d09-be3a-afb5c438bc8d
Rahul, A., Arya, H. K., and Saxena, R. K. (2014). Effect of cooling rate on microstructure of SAW welded mild steel plate (Grade C 25 as Per IS 1570). International Journal of Modern Engineering Research, 4(1), 222-228.
Rosenthal, D. (1941). Mathematical theory of heat distribution during welding and cutting. Welding journal, 20(5), 220s-234s.
Rosenthal, D. (1946). The theory of moving sources of heat and its application to metal treatments. Transactions of the American Society of Mechanical Engineers, 68(8), 849-865.
Rothwell, J. S., and Abson, D. J. (2013). The effect of thermal history during fabrication on the mechanical properties of weldments in grade 91 creep resistant steel. Welding in the World, 57(6), 913-924. https://doi.org/10.1007/s40194-013-0085-8
Sarkar, A. (2015). A numerical approach for modelling thermal profiles and effects of process parameters on it in submerged arc welding of AISI 1518 grade steel. Journal of Thermal Engineering, 1(6). https://doi.org/10.18186/jte.55588
Sarkar, A., Rai, R. N., and Saha, S. C. (2015). A study of parametric effects on thermal profile of submerged arc welding process. Journal of Naval Architecture and Marine Engineering, 12(1), 43-56. https://doi.org/10.3329/jname.v12i1.22670
Sharir, Y., Grill, A., and Pelleg, J. (1980). Computation of temperatures in thin tantalum sheet welding. Metallurgical Transactions B, 11(2), 257-265. https://doi.org/10.1007/BF02668410
Tarng YS, Juang SC, Chang CH (2002). The use of grey-based Taguchi methods to determine submerged arc welding process parameters in hard facing. J Mater Process Technol 128:1-6 https://doi.org/10.1016/S0924-0136(01)01261-4
Yaghi, A. H., Hyde, T. H., Becker, A. A., and Sun, W. (2009). Thermo-mechanical modelling of weld microstructure and residual stresses in P91 steel pipe. Energy Materials, 4(3), 113-123. https://doi.org/10.1179/174892310X12779109287084
Yaghi, A. H., Hyde, T. H., Becker, A. A., and Sun, W. (2008). Finite element simulation of welding and residual stresses in a P91 steel pipe incorporating solid-state phase transformation and post-weld heat treatment. The Journal of Strain Analysis for Engineering Design, 43(5), 275-293. https://doi.org/10.1243/03093247JSA372
Yaghi, A. H., Hyde, T. H., Becker, A. A., Sun, W., Hilson, G., Simandjuntak, S., and Smith, D. J. (2009, April). Measuring and modelling residual stresses in a butt-welded P91 steel pipe. In 2009 International Conference on Sustainable Power Generation and Supply (pp. 1-5). IEEE. https://doi.org/10.1109/SUPERGEN.2009.5348017
Yeh, R. H., Liaw, S. P., and Yu, H. B. (2003). Thermal analysis of welding on aluminum plates. Journal of Marine Science and Technology, 11(4), 5. https://doi.org/10.51400/2709-6998.2292
Zubairuddin, M., Albert, S. K., Vasudevan, M., Chaudhari, V., and Suri, V. K. (2014). Finite element simulation of weld bead geometry and temperature distribution during GTA welding of modified 9Cr-1Mo steel and experimental validation. Journal for Manufacturing Science and Production, 14(4), 195-207. https://doi.org/10.1515/jmsp-2014-0006;
Zubairuddin, M., Vasudevan, M., Das, P. K., Alam, M. M., Kumar, K. S., and Prabhakar, S. (2025). FEM based thermal and mechanical analysis of comparative study of TIG and A-TIG welding on P91 steel. Scientific Reports, 15(1), 10271. https://doi.org/10.1038/s41598-025-90998-x
Zubairuddin, M., Vasudevan, M., Elumalai, P. V., Akram, M., Attar, P. R., and Krishnasamy, E. (2024). "Numerical and experimental analysis of temperature and residual stress of GTA and LASER welding for grade 91 steel". International Journal on Interactive Design and Manufacturing (IJIDeM), 1-13. https://doi.org/10.1007/s12008-024-02138-w